Finite States Model Predictive Control for Fault-Tolerant Operation of a Three-Phase Bidirectional AC/DC Converter Under Unbalanced Grid Voltages

Nan Jin ⓘ, *Member, IEEE*, Shiyang Hu ⓘ, Chun Gan ⓘ, *Member, IEEE*, and Zhibin Ling ⓘ, *Member, IEEE*

Abstract—The bidirectional ac/dc converter is widely used to realize the power conversion between ac and dc microgrid, but the faults of switch devices and unbalanced grid voltages may lead to the decline of power quality and affect normal operation of the converter. The four-switch three-phase (FSTP) fault-tolerant structure is reconstructed from a six-switch three-phase structure with switch device fault. In order to reduce harmonic currents and output power fluctuations under unbalanced grid voltages, finite states model predictive direct power control (MPDPC) with power compensation method is proposed for FSTP structure and predictive power model of the bidirectional FSTP ac/dc converter is established. The power compensation values are expressed by grid voltages and their quadrature signals that lagging 90 electrical degrees in the $\alpha\beta$ stationary coordinate system. Compared with the conventional method, phase-locked loop, pulse width modulation, and complex positive-/negative-sequence extraction of grid voltage are not required. Ripples of active power or reactive power under unbalanced grid voltages are eliminated. The proposed fault-tolerant MPDPC with power compensation method ensures the continuous and reliable operation of the bidirectional ac/dc converter with high power quality. Simulation and experimental results are presented to validate the proposed control strategy under symmetrical unbalanced grid voltages with switch device faults.

Index Terms—Bidirectional ac/dc converter, fault-tolerant control, four switch three phase (FSTP), model predictive direct power control (MPDPC), unbalanced grid voltages.

I. INTRODUCTION

THE reliability and fault-tolerant operation ability of a large-capacity power conversion system is not only the primary basis for power electronic device operation, but also the premise and basis to build a strong smart grid [1], [2]. As the link and key equipment in the hybrid microgrid, bidirectional ac/dc converter controls bidirectional power flow between dc bus and ac grid, which plays an important role in reliable operation of the microgrids [3]–[5]. As the core component of the hybrid microgrids to control power conversion, the normal operation of a bidirectional ac/dc converter is the basis of the whole system. The fault of converter results in disconnection between the dc microgrids and ac microgrids, which has a great impact on the grid and threatens the safety and stable operation of the power grid and reliable power supply of important users. However, power electronics switching devices are usually used in occasions like high voltage, large capacity, and high power density. They are prone to have faults caused by surges of voltage or current in high-frequency switching transient process [6]–[8]. Therefore, it is of great significance to study the fault-tolerance mechanism and control method of a bidirectional ac/dc converter to improve the reliability.

Bidirectional ac/dc converter is widely used in hybrid microgrids, energy storage power converter, motor control, and other fields. It has the ability to realize bidirectional power flow between ac and dc power system [4], [9], [10]. However, the switching devices of converter are inevitably damaged in high-frequency and large-capacity power conversion. The consequences are serious and becoming a danger threat to the reliability of microgrids. In addition, the harmonic contents of grid current and twice grid-frequency ripples in output power increase significantly under unbalanced grid voltages, which decrease the power quality of a converter. It is necessary to design control strategy of a bidirectional ac/dc converter under unbalanced grid voltages with switching device faults.

In order to improve the fault-tolerance ability of a power converter, the fault-tolerant structure and the corresponding control strategy are combined to maintain the continuous operation of a power converter when there is a fault. At present, fault-tolerance methods have been studied in unidirectional power conversion fields, such as motor control, pulse width

modulation (PWM) rectifier, and grid-connected inverter [11]–[16]. The four-switch three-phase (FSTP) converter which is tolerant structure of six-switch three-phase (SSTP) converter can enhance the system reliability, maintain continuous operation ability with one bridge arm failure. Compared with six-switch converter, the four-switch converter can reduce the switching frequency, power losses, and cost.

A vector PWM strategy for FSTP inverters is proposed [8], [14]. It offers a method to select three or four vectors by space vector modulation. Compared with the standard SSTP inverter, the proposed approach shows feasibility performance. A sine-wave PWM control strategy is proposed for FSTP inverter topology instead of the traditional complex four-switches-based space vector techniques. A novel design for the FSTP inverter based on the topology of the single-ended primary-inductance converter is presented in [15]. It provides pure sinusoidal output voltages with no output filter and improve the voltage utilization factor of the input dc supply. These fault-tolerant methods of an FSTP converter are based on the PWM control method, which needs coordinate transform and modulation signals with the complex algorithms. However, these methods have not considered fault-tolerant control of bidirectional ac/dc converter and the operation process is complex.

The conventional control methods of bidirectional ac/dc converter generate control signals using PWM. A simplified PWM control scheme with switching constraints was also designed, which can reduce the circulating current of the parallel bidirectional ac/dc converter without additional current sensor and communication equipment [4]. Both the dc voltage and the ac current can be controlled only by the voltage loop. A three-phase isolated bidirectional ac/dc converter, which modified the space vector pulse width modulation (SVPWM) algorithm to realize the bidirectional buck–boost converter, was proposed in [5]. The method can maintain the current sinusoidal and high-frequency electrical isolation. A new bus voltage control technology was proposed for the single-phase bidirectional ac/dc converter [9], which can significantly improve the transient response of the bus voltage control and establish a reliable closed-loop control system. The external voltage loop controls dc voltage and the inner current loop controls grid current. A bidirectional current sensorless control strategy based on a field-programmable gate array (FPGA) control system was designed in [17]. A novel simplified PWM control strategy for a bidirectional ac/dc converter was proposed in [18], which is better than the traditional double-loop control with feedforward control.

The unbalanced ac voltages have been proven to be one of the greatest challenges for the control of the converter in order to keep them normally operating and connected to the ac source. Special control methods which can regulate both the positive- and negative-sequence currents have been introduced to handle these problems [19], [20]. Power compensations are added to the reference active or reactive power to improve the performance using direct power control (DPC) [21], [22], but they still require positive-/negative-sequence separations. Approaches of improved model predictive direct power control (MPDPC) for PWM rectifiers were proposed in [23]. The first approach achieves low switching frequency, whereas the

second approach obtains lower power ripples. A low-complexity MPDPC with power compensation (MPDPC-PC) strategy for doubly-fed induction generator under both balanced and unbalanced grid conditions was proposed in [24]. Phase-locked loop (PLL) and sequence extraction are required. The DPC is a kind of high-performance control strategy for the PWM converter. However, the switching table in conventional DPC is obtained in a heuristic way, which cannot assure the effectiveness of the selected voltage vector [25], [26].

Most researches are focused on the control in normal condition without fault-tolerant operation. These methods do not consider the fault-tolerant control of FSTP bidirectional ac/dc converter under unbalanced grid circumstances. It is necessary to try new control strategy of a bidirectional ac/dc converter with leg faults. As an intitutive control strategy, model predictive control (MPC) is applied for power converters. It has good adaptability and robustness without inner loop current control and PWM modulation [27]–[33]. A MPDPC strategy is presented for a grid-connected inverter used in photovoltaic system [34]. A sliding-mode-based preselection step that limits the prediction process and a table-based implementation process are used to reduce the execution time of the whole control algorithm [35]. Prediction model is used to calculate inverter behavior at each sampling instant. The optimal voltage vector is selected by a cost function and applied during the next sampling period to achieve the least power ripple. The inverter works properly without any fault. Once the bridge leg of converter has a short-circuit or open-circuit fault, the MPDPC method performance needs to be improved.

In this paper, the working mechanism of a high-reliability FSTP bidirectional ac/dc converter is analyzed and its power predictive model is established. Finite states MPDPC method for FSTP bidirectional ac/dc converter under unbalanced grid voltage is proposed. The finite states MPC is widely used because of its accurate and effective selection of voltage vector. By selecting the best voltage vector to minimize the cost function, the MPDPC method shows good steady state and dynamic performance. Output power is expressed with grid voltage/current and their lagging signals, which is different from the conventional expression using the positive- and negative-sequence components. The bidirectional ac/dc converter is controlled under unbalanced grid voltages by adding compensation power to the reference power. The compensation power is calculated using grid voltage/current in $\alpha\beta$ stationary coordinate system and their 90° lagging signals. Without the Park transform, extraction of current positive-/negative-sequence components and PLL, the harmonic contents of grid current are reduced and active power or reactive power ripples are eliminated using the proposed MPDPC-PC. The flexible seamless switching between the inverter and rectifier mode of bidirectional ac/dc converter is achieved by changing the reference active power. The proposed method can realize fault-tolerant continuous operation of bidirectional ac/dc converter and eliminate active power or reactive power ripples under unbalanced grid voltages with sinusoidal current waveforms. Simulation and experiment results verify the effectiveness of the designed control strategy.
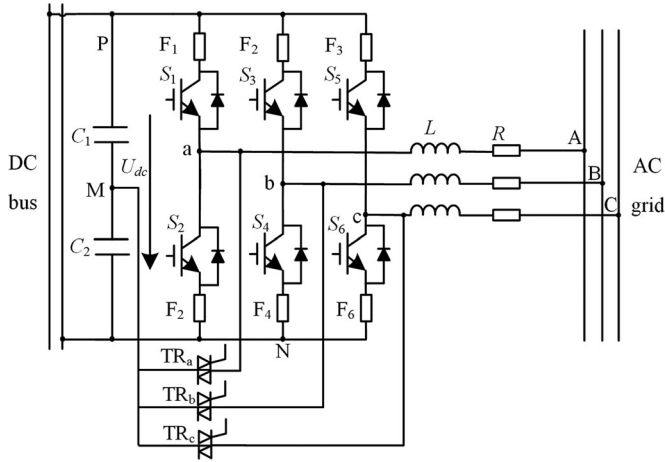
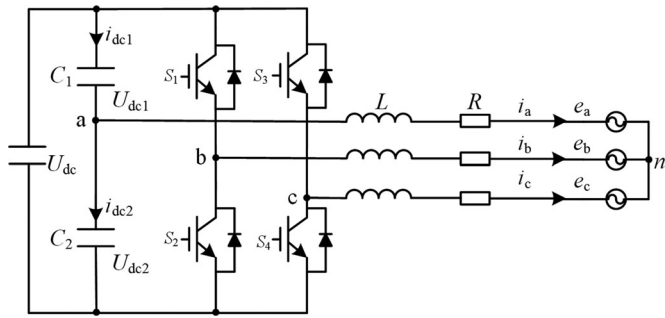Fig. 1.   Fault-tolerant topology of a bidirectional ac/dc converter.

Fig. 2.   Bidirectional FSTP ac/dc converter.

II. FAULT-TOLERANT FSTP POWER PREDICTIVE MODEL

The common fault types of bidirectional ac/dc converter include ground short of dc bus, short circuit of dc capacitor, trigger pulse loss of power devices, short circuit of power device, open circuit of power device, short circuit of inverter bridge, open circuit of ac side, phase-to-phase short circuit, and ground short of single phase [8], [11]–[13]. In this paper, the fault-tolerant control of bidirectional ac/dc converter with open circuit and short circuit of power device is studied. The short-circuit time of the power device is usually very short (less than 10 μs). Hence, it is usually in series fast fuse device with the bridge leg and converted short-circuit fault to open-circuit fault.

The fault-tolerant structure of a bidirectional ac/dc converter is shown in Fig. 1, which is connected with central point of the series capacitor by bidirectional thyristors (TR_a, TR_b, TR_c). In normal operation, the bidirectional thyristor is in the open state. When the short circuit or open circuit occur in one bridge leg (such as phase A), fast fuse device (F_1 or F_2) is opened and the corresponding bidirectional thyristor tube TR_a is conducted to achieve continuous operation [8]. The reconstructed FSTP bidirectional ac/dc converter is shown in Fig. 2.

The FSTP converter topology with phase *A* fault is shown in Fig. 2. According to Kirchhoffs law, the state equation of the converter in *abc* three-phase static coordinate system is obtained

$$L\frac{\mathrm{d}}{\mathrm{d}t}\begin{bmatrix} i_a \\ i_b \\ i_c \end{bmatrix} + R\begin{bmatrix} i_a \\ i_b \\ i_c \end{bmatrix} = \begin{bmatrix} u_{an} \\ u_{bn} \\ u_{cn} \end{bmatrix} - \begin{bmatrix} e_a \\ e_b \\ e_c \end{bmatrix} \tag{1}$$

where u_{an}, u_{bn}, u_{cn} are output three-phase voltages of converter, i_a, i_b, i_c are output three-phase currents of converter, and e_a, e_b, e_c are three-phase grid voltages.

The state equation of the $\alpha\beta$ two-phase stationary coordinates is obtained by Clark transform of (1) as

$$L\frac{d}{dt}\begin{bmatrix} i_\alpha \\ i_\beta \end{bmatrix} + R\begin{bmatrix} i_\alpha \\ i_\beta \end{bmatrix} = \begin{bmatrix} u_\alpha \\ u_\beta \end{bmatrix} - \begin{bmatrix} e_\alpha \\ e_\beta \end{bmatrix} \tag{2}$$

where $i_\alpha, i_\beta, u_\alpha, u_\beta, e_\alpha, e_\beta$ are the $\alpha\beta$ components of converter output current, voltage, and power grid voltage, respectively.

The switching state S_i ($i = $ b, c) of a fault-tolerant grid-connected converter is defined as follows:

$$S_i = $$

$$\begin{cases} 1 & \text{upper bridge of phase } i \text{ is on and lower bridge is off} \\ 0 & \text{upper bridge of phase } i \text{ is off and lower bridge is on} \end{cases}. \tag{3}$$

The relation expression between the output voltage and the switching state of FSTP converter is

$$\begin{bmatrix} u_{an} \\ u_{bn} \\ u_{cn} \end{bmatrix} = \frac{U_{\mathrm{dc}}}{3}\begin{bmatrix} 2 & -1 & -1 \\ -1 & 2 & -1 \\ -1 & -1 & 2 \end{bmatrix}\begin{bmatrix} 1/2 \\ Sb \\ Sc \end{bmatrix}. \tag{4}$$

The state equation of the $\alpha\beta$ two-phase stationary coordinates is obtained by Clark transform of (4)

$$\begin{bmatrix} u_\alpha \\ u_\beta \end{bmatrix} = \frac{2U_{\mathrm{dc}}}{9}\begin{bmatrix} 1 & -\dfrac{1}{2} & -\dfrac{1}{2} \\ 0 & \dfrac{\sqrt{3}}{2} & -\dfrac{\sqrt{3}}{2} \end{bmatrix}\begin{bmatrix} 1 - S_b - S_c \\ -1/2 + 2S_b - S_c \\ -1/2 - S_b + 2S_c \end{bmatrix}. \tag{5}$$

Space voltage vector of FSTP structure is defined as

$$\boldsymbol{U}_{\mathrm{out}} = \frac{2}{3}\left(u_{an} + au_{bn} + a^2 u_{cn}\right) \tag{6}$$

where $a = \mathrm{e}^{j2\pi/3}$ is the rotation factor.

FSTP converter has four switching states of (0 0), (0 1), (1 0), (1 1). The output voltage vectors with switch fault are shown in Table I.

The voltage vectors divide the vector space into four sectors, which are shown in Fig. 3. Obviously, the amplitude of the 4 basic voltage vectors are not equal.

Formula (2) is discretized as

$$\frac{L}{T_s}\begin{bmatrix} i_\alpha(k+1) - i_\alpha(k) \\ i_\beta(k+1) - i_\beta(k) \end{bmatrix} = \begin{bmatrix} u_\alpha(k) \\ u_\beta(k) \end{bmatrix} - R\begin{bmatrix} i_\alpha(k) \\ i_\beta(k) \end{bmatrix} - \begin{bmatrix} e_\alpha(k) \\ e_\beta(k) \end{bmatrix} \tag{7}$$

where T_s is the sampling period.

Simplify (7), the predictive current at t_{k+1} instant is given as follows:

$$\begin{bmatrix} i_\alpha(k+1) \\ i_\beta(k+1) \end{bmatrix} = \frac{T_s}{L}\begin{bmatrix} u_\alpha(k) - e_\alpha(k) \\ u_\beta(k) - e_\beta(k) \end{bmatrix} + \left(1 - \frac{RT_s}{L}\right)\begin{bmatrix} i_\alpha(k) \\ i_\beta(k) \end{bmatrix} \tag{8}$$

TABLE I
VOLTAGE VECTORS WITH SWITCH FAULT

$U(S_b, S_c)$	u_α	u_β	U_{out}
$U_0(0,0)$	$U_{dc}/3$	0	$U_{dc}/3$
$U_1(0,1)$	0	$-\sqrt{3}U_{dc}/3$	$\sqrt{3}U_{dc}e^{j3\pi/2}/3$
$U_2(1,0)$	0	$\sqrt{3}U_{dc}/3$	$\sqrt{3}U_{dc}e^{j\pi/2}/3$
$U_3(1,1)$	$-U_{dc}/3$	0	$-U_{dc}/3$

(a) Phase A Switch Fault

$U(S_a, S_c)$	u_α	u_β	U_{out}
$U_0(0,0)$	$-U_{dc}/6$	$\sqrt{3}U_{dc}/6$	$U_{dc}e^{j2\pi/3}/3$
$U_1(0,1)$	$-U_{dc}/2$	$-\sqrt{3}U_{dc}/6$	$\sqrt{3}U_{dc}e^{j7\pi/6}/3$
$U_2(1,0)$	$U_{dc}/2$	$\sqrt{3}U_{dc}/6$	$\sqrt{3}U_{dc}e^{j\pi/6}/3$
$U_3(1,1)$	$U_{dc}/6$	$-\sqrt{3}U_{dc}/6$	$U_{dc}e^{j5\pi/3}/3$

(b) Phase B Switch Fault

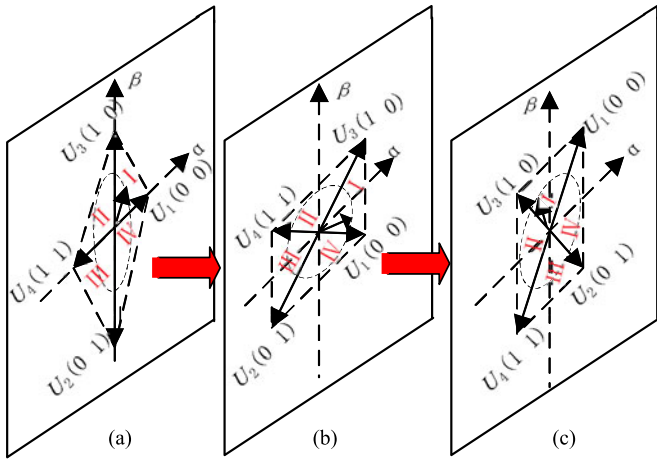| $U(S_a, S_b)$	u_α	u_β	U_{out}
$U_0(0,0)$	$-U_{dc}/6$	$-\sqrt{3}U_{dc}/6$	$U_{dc}e^{j4\pi/3}/3$
$U_1(0,1)$	$-U_{dc}/2$	$\sqrt{3}U_{dc}/6$	$\sqrt{3}U_{dc}e^{j5\pi/6}/3$
$U_2(1,0)$	$U_{dc}/2$	$-\sqrt{3}U_{dc}/6$	$\sqrt{3}U_{dc}e^{j11\pi/6}/3$
$U_3(1,1)$	$U_{dc}/6$	$\sqrt{3}U_{dc}/6$	$U_{dc}e^{j\pi/3}/3$

(c) Phase C Switch Fault

Fig. 3. Voltage space vectors: (a) Phase A switch fault, (b) phase B switch fault, and (c) phase C switch fault.

where $i_\alpha(k)$, $i_\beta(k)$, $u_\alpha(k)$, $u_\beta(k)$, $e_\alpha(k)$, $e_\beta(k)$ are $\alpha\beta$ components of the converter output current, voltage, and the grid voltage at t_k instant, respectively. $i_\alpha(k+1)$ and $i_\beta(k+1)$ are $\alpha\beta$ components of predictive current value at t_{k+1} instant.

According to the instantaneous power theory, the output active and reactive power of the converter can be expressed as

$$\begin{cases} p = e_\alpha i_\alpha + e_\beta i_\beta \\ q = e_\beta i_\alpha - e_\alpha i_\beta \end{cases}. \tag{9}$$

Under the condition of high sampling frequency, the following assumption can be made:

$$\begin{cases} e_\alpha(k+1) = e_\alpha(k) \\ e_\beta(k+1) = e_\beta(k) \end{cases}. \tag{10}$$

Substituting (10) into (9), the predictive power model of t_{k+1} instant is

$$\begin{cases} p(k+1) = e_\alpha(k)i_\alpha(k+1) + e_\beta(k)i_\beta(k+1) \\ q(k+1) = e_\beta(k)i_\alpha(k+1) - e_\alpha(k)i_\beta(k+1) \end{cases}. \tag{11}$$

III. POWER ANALYSIS AND COMPENSATION UNDER UNBALANCED GRID VOLTAGE

Under unbalanced grid voltages, positive- and negative-sequence components are extracted from the grid voltages and currents [19], [20]. The active power and reactive power of the converter will contain power ripples with twice grid frequency. In traditional PWM control, the PLL technology was used to separate the positive- and negative-sequence of voltage and current. The calculation amount is large and the control strategy is complex. A method to express active power and reactive power by grid voltages and currents with their quadrature signals [21]. Therefore, without extraction of sequence components, the method is easier to realize. However, it mainly achieves constant active power from dc to ac side. The method is extended for bidirectional ac/dc converter to achieve bidirectional energy conversion between ac and dc sides with switch fault, and the elimination of reactive power ripples is also realized.

A. Conventional Power Analysis in a dq Coordinate System

In unbalanced grid, voltage and current can be expressed as the sum of positive- and negative-sequence components [19]

$$\begin{cases} e = e_{\alpha\beta}^+ + e_{\alpha\beta}^- = e_{dq}^+ e^{j\omega t} + e_{dq}^- e^{-j\omega t} \\ i = i_{\alpha\beta}^+ + i_{\alpha\beta}^- = i_{dq}^+ e^{j\omega t} + i_{dq}^- e^{-j\omega t} \end{cases} \tag{12}$$

where

$$\begin{cases} e_{dq}^+ = e_d^+ + je_q^+ \\ e_{dq}^- = e_d^- + je_q^- \\ i_{dq}^+ = i_d^+ + ji_q^+ \\ i_{dq}^- = i_d^- + ji_q^- \end{cases} \tag{13}$$

where $e_{\alpha\beta}^+$, $e_{\alpha\beta}^-$, e_{dq}^+, e_{dq}^-, $i_{\alpha\beta}^+$, $i_{\alpha\beta}^-$, i_{dq}^+, i_{dq}^- are the positive- and negative-sequence components of the grid voltage and current in the $\alpha\beta$ stationary coordinate system and the dq rotating coordinate system; ω is the angular frequency.

The power of grid side can be expressed by the positive- and negative-sequence components of voltage and current

$$S = ei^* = (e_{dq}^+ e^{j\omega t} + e_{dq}^- e^{-j\omega t})(i_{dq}^+ e^{j\omega t} + i_{dq}^- e^{-j\omega t})^* = p + jq \tag{14}$$

where

$$\begin{cases} p = p_0 + p_{c2}\cos(2\omega t) + p_{s2}\sin(2\omega t) \\ q = q_0 + q_{c2}\cos(2\omega t) + q_{s2}\sin(2\omega t) \end{cases}. \tag{15}$$

Reorganizing (14) and (15), the expression of active power and reactive power in dq rotating coordinate can be obtained

by

$$
\begin{cases}
p_0 = e_d^+ i_d^+ + e_q^+ i_q^+ + e_d^- i_d^- + e_q^- i_q^- \\
p_{c2} = e_d^+ i_d^- + e_q^+ i_q^- + e_d^- i_d^+ + e_q^- i_q^+ \\
p_{s2} = e_q^+ i_d^- - e_d^+ i_q^- + e_d^- i_q^+ - e_q^- i_d^+ \\
q_0 = e_q^+ i_d^+ - e_d^+ i_q^+ + e_q^- i_d^- - e_d^- i_q^- \\
q_{c2} = e_q^+ i_d^- - e_d^+ i_q^- + e_q^- i_d^+ - e_d^- i_q^+ \\
q_{s2} = e_d^+ i_d^- + e_q^+ i_q^- - e_d^- i_d^+ - e_q^- i_q^+
\end{cases} \tag{16}
$$

where p_{c2}, p_{s2}, q_{c2}, and q_{s2} are the ripples of active power and reactive power, respectively, and p_0 and q_0 are the average value.

B. Power Analysis in a $\alpha\beta$ Coordinate System

Supposed x is variable in $\alpha\beta$ stationary coordinate, then the quadrature signals that lagging 90° can be expressed as x'. The relationship between positive- and negative-sequence components with quadrature signal is

$$
x' = x_{\alpha\beta}^{+\prime} + x_{\alpha\beta}^{-\prime} = x_{dq}^+ e^{j(\omega t - \frac{\pi}{2})} + x_{dq}^- e^{-j(\omega t - \frac{\pi}{2})}
$$
$$
= -j x_{dq}^+ e^{j\omega t} + j x_{dq}^- e^{-j\omega t} = -j x_{\alpha\beta}^+ + j x_{\alpha\beta}^-. \tag{17}
$$

The expression corresponding to x' is

$$
x' = x_{\alpha\beta}^{+\prime} + x_{\alpha\beta}^{-\prime} = -j x_{\alpha\beta}^+ + j x_{\alpha\beta}^-. \tag{18}
$$

Then, the relationship between x, x' and sequence component $x_{\alpha\beta}^+$, $x_{\alpha\beta}^-$ in stationary coordinates are expressed as

$$
\begin{bmatrix} x \\ x\prime \end{bmatrix} = \begin{bmatrix} 1 & 1 \\ -j & j \end{bmatrix} \begin{bmatrix} x_{\alpha\beta}^+ \\ x_{\alpha\beta}^- \end{bmatrix}. \tag{19}
$$

The inverse of (19) can be obtained

$$
\begin{bmatrix} x_{\alpha\beta}^+ \\ x_{\alpha\beta}^- \end{bmatrix} = \frac{1}{2} \begin{bmatrix} 1 & j \\ 1 & -j \end{bmatrix} \begin{bmatrix} x \\ x' \end{bmatrix}. \tag{20}
$$

The relationship between positive- and negative-sequence components in dq rotating coordinate system and $\alpha\beta$ stationary coordinate system is

$$
\begin{bmatrix} x_{dq}^+ \\ x_{dq}^- \end{bmatrix} = \begin{bmatrix} e^{-j\omega t} & 0 \\ 0 & e^{j\omega t} \end{bmatrix} \begin{bmatrix} x_{\alpha\beta}^+ \\ x_{\alpha\beta}^- \end{bmatrix}. \tag{21}
$$

From (20) and (21), the relationship between positive-/negative-sequence components in dq rotating coordinate and $\alpha\beta$ stationary coordinate variables delay signal is

$$
\begin{bmatrix} x_{dq}^+ \\ x_{dq}^- \end{bmatrix} = \frac{1}{2} \begin{bmatrix} e^{-j\omega t} & j e^{-j\omega t} \\ e^{j\omega t} & -j e^{j\omega t} \end{bmatrix} \begin{bmatrix} x \\ x' \end{bmatrix}. \tag{22}
$$

Substituting (22) into (16), active power and reactive power is expressed by $\alpha\beta$ static coordinate system voltage, current, and

their respective lagging signals

$$
\begin{cases}
p_0 = \frac{1}{2}(i_\alpha e_\alpha + i_\beta e_\beta + i_\alpha' e_\alpha' + i_\beta' e_\beta') \\
p_{c2} = \frac{1}{2}\left[k_1 \cos(2\omega t) + k_2 \sin(2\omega t) \right] \\
p_{s2} = \frac{1}{2}\left[-k_2 \cos(2\omega t) + k_1 \sin(2\omega t) \right] \\
q_0 = \frac{1}{2}(i_\alpha e_\beta - i_\beta e_\alpha + i_\alpha' e_\beta' - i_\beta' e_\alpha') \\
q_{c2} = \frac{1}{2}\left[k_3 \cos(2\omega t) + k_4 \sin(2\omega t) \right] \\
q_{s2} = \frac{1}{2}\left[-k_4 \cos(2\omega t) + k_3 \sin(2\omega t) \right]
\end{cases} \tag{23}
$$

where

$$
\begin{cases}
k_1 = i_\alpha e_\alpha + i_\beta e_\beta - i_\alpha' e_\alpha' - i_\beta' e_\beta' \\
k_2 = i_\alpha e_\alpha' + i_\beta e_\beta' + i_\alpha' e_\alpha + i_\beta' e_\beta \\
k_3 = i_\alpha e_\beta - i_\beta e_\alpha - i_\alpha' e_\beta' + i_\beta' e_\alpha' \\
k_4 = i_\alpha e_\beta' - i_\beta e_\alpha' + i_\alpha' e_\beta - i_\beta' e_\alpha
\end{cases} \tag{24}
$$

where i_α, i_β, e_α, e_β, i_α', i_β', e_α', e_β' are the $\alpha\beta$ components of grid current, voltage, and their 90° lagging signals, respectively. p_{c2}, p_{s2}, q_{c2}, q_{s2} are the fluctuation components of the active power and reactive power, respectively.

C. Power Compensation I: Eliminating Ripples in Active Power

According to (23), there are eight parameters (i_α, i_β, i_α', i_β', e_α, e_β, e_α', e_β'). By using e_α, e_β, e_α', e_β' to express i_α, i_β, i_α', i_β', the new reference current i_{ref} value is solved. Therefore, four formulas in (23) are needed to obtain i_{ref}.

In order to eliminate the active power pulsation, the p_{c2} and p_{s2} in (23) are zero. k_1 and k_2 are zero. The control objective is equivalent to solve the following equation:

$$
\begin{cases}
p_0 = p_{\text{ref}} \\
q_0 = 0 \\
k_1 = 0 \\
k_2 = 0
\end{cases}. \tag{25}
$$

Then, a new reference current value in $\alpha\beta$ stationary coordinates is shown as follows:

$$
i_{\text{new}}^{\text{ref}} = i_\alpha + j i_\beta = \frac{p_{\text{ref}}(e_\beta' - j e_\alpha')}{e_\alpha e_\beta' - e_\alpha' e_\beta}. \tag{26}
$$

Hence, the power compensation value should be the error between new power reference value and the original power reference value, given by

$$
S^{\text{comp}} = S_{\text{new}}^{\text{ref}} - S^{\text{ref}} = j\frac{e_\alpha e_\alpha' + e_\beta e_\beta'}{e_\alpha e_\beta' - e_\alpha' e_\beta} p_{\text{ref}}. \tag{27}
$$

The compensation value of active power and reactive power is obtained by

$$
\begin{cases}
p_{\text{comp}}(k+1) = 0 \\
q_{\text{comp}}(k+1) = \frac{e_\alpha e_\alpha' + e_\beta e_\beta'}{e_\alpha e_\beta' - e_\alpha' e_\beta} p_{ref}
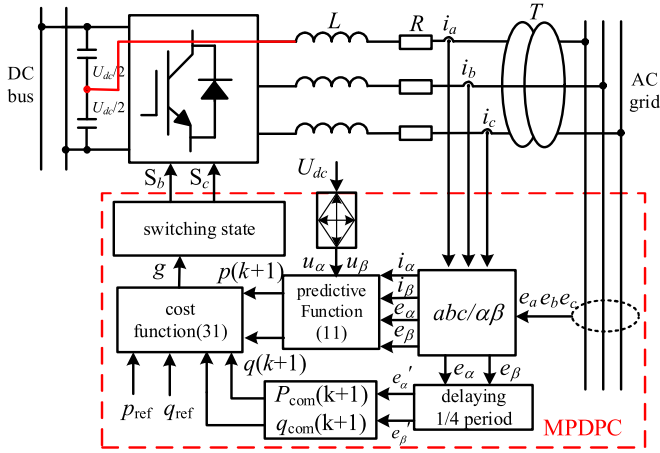\end{cases}. \tag{28}
$$

Fig. 4.   Control structure of a fault-tolerant FSTP bidirectional ac/dc converter.

D. Power Compensation II: Eliminating Ripples in Reactive Power

In order to eliminate the reactive power pulsation, q_{c2} and q_{s2} in (23) are zero. So k_3 and k_4 are zero. The control objective is equivalent to solve the following equations:

$$\begin{cases} p_0 = p_{\text{ref}} \\ q_0 = 0 \\ k_3 = 0 \\ k_4 = 0 \end{cases}. \tag{29}$$

The corresponding power compensation value of active power and reactive power is obtained by

$$\begin{cases} p_{\text{comp}}(k+1) = \dfrac{e_\alpha{}^2 + e_\beta{}^2 - e_\alpha'{}^2 - e_\beta'{}^2}{e_\alpha{}^2 + e_\beta{}^2 + e_\alpha'{}^2 + e_\beta'{}^2} p_{ref} \\ q_{\text{comp}}(k+1) = 0 \end{cases}. \tag{30}$$

IV. MPDPC STRATEGY WITH POWER COMPENSATION

A. Proposed MPDPC-PC for an FSTP AC/DC converter

Without the traditional extraction of positive- and negative-sequence control, voltage, and current in the $\alpha\beta$ stationary coordinate system with their 90° lagging signals can express power compensation value. MPDPC with power compensation strategy is proposed to control the bidirectional ac/dc converter.

In order to select the optimal switching vector and realize the DPC, the cost function g is established as follows:

$$g = |p_{\text{ref}} + p_{\text{com}}(k+1) - p(k+1)|$$
$$+ |q_{\text{ref}} + q_{\text{com}}(k+1) - q(k+1)| \tag{31}$$

where p_{ref}, q_{ref} are active power, reactive power reference values. $p_{\text{com}}(k+1)$, $q_{\text{com}}(k+1)$, $p(k+1)$, $q(k+1)$ are power compensation and prediction values at t_{k+1} instant.

MPDPC control structure of fault-tolerant operation with power compensation is shown in Fig. 4. First, grid voltage and current e_a, e_b, e_c, i_a, i_b, i_c are sampled. e_α, e_β, i_α, i_β are obtained in the $\alpha\beta$ stationary coordinate system with Clark transform. e_α', e_β' are obtained by 90° lagging and power
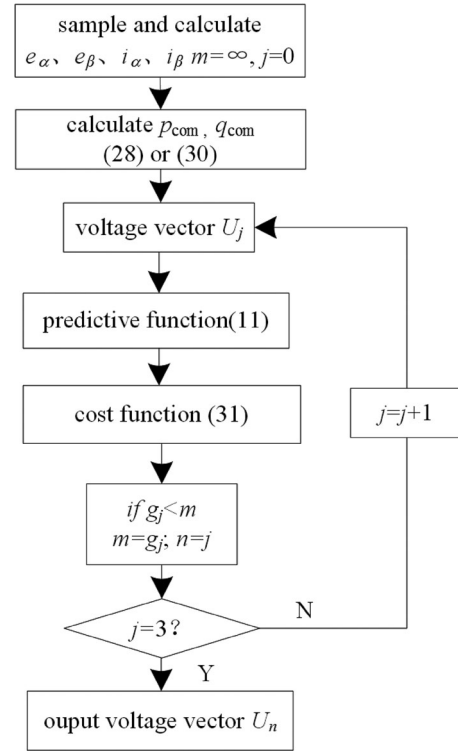

Fig. 5.   Flow diagram of MPDPC with power compensation.

TABLE II
SYSTEM PARAMETERS COMPARING OF EXISTING AND PROPOSED SCHEMES

	SVPWM [8], [14], [19]	DPC [25], [26]	MPDPC [27]–[33]	Proposed FSTP-MPDPC
Fault-tolerant capability	Yes	No	No	Yes
d-q transformation	Required	Required	Not Required	Not Required
Current distortion	Low	Medium	High	Low
PLL	Required	Required	Not Required	Not Required
Power Ripple	Medium	Low	High	Low
Sequence extraction	Required	Required	Not Required	Not Required

compensation values $p_{\text{com}}(k+1)$, $q_{\text{com}}(k+1)$ are calculated. The output voltages of converter u_α, u_β are obtained by U_{dc}. Predictive function (11) outputs power predictive value $p(k+1)$, $q(k+1)$. The cost function (31) is used to evaluate the voltage vectors, then the switching state S_{a}, S_{b}, S_{c} which minimize the cost function is selected and applied at t_{k+1} instant to achieve DPC. Flow diagram of MPDPC with power compensation algorithm is shown in Fig. 5.

B. Comparison of the Existing and Proposed Schemes

A detailed comparison of the proposed schemes with existing methods is presented in Table II.

The DPC is a high-performance control strategy for the PWM converter [25], which is similar to the direct torque control in motor drives. Compared to the voltage-oriented control, the DPC directly selects the desired voltage vector from a predefined switching table and eliminates the internal current loop.

As a result, the dynamic response is very quick. However, the switching table in conventional DPC is obtained in a heuristic way, which cannot assure the effectiveness of the selected voltage vector. As a result, Zhang and Zhu have revised the conventional switching table to achieve performance improvement by proposing new switching tables [26]. However, the performance improvement is limited, because the complete model of the PWM converter and its future behavior are not taken into account.

The MPDPC is similar to the DPC in that they both select one voltage vector for the next control period, but their vector selection principles are very different. In the MPDPC, the complete model and future behavior of the PWM converter are taken into account. A cost function relating to power errors reduction is defined to evaluate the effects of each voltage vector and the one minimizing the cost function is selected. Compared to the switching table in DPC, the vector selected from the MPDPC is more accurate and effective in reducing power errors.

Under unbalanced grid-voltage conditions, control schemes which can regulate both the positive- and negative sequence currents have been introduced to handle these problems [19]. Power compensations are added to the reference active or reactive power to improve the performance using DPC [21], but they still require positive-/negative-sequence separations.

The FSTP fault-tolerant structure is reconstructed from SSTP structure with switch device fault. In order to reduce harmonic currents and output power fluctuations under unbalanced grid voltages, finite states MPDPC with power compensation method is proposed for FSTP structure and predictive power model of the bidirectional FSTP ac/dc converter is established. The power compensation values are expressed by grid voltages and their quadrature signals that lagging 90 electrical degrees in the $\alpha\beta$ stationary coordinate system. Compared with the conventional method, PLL, PWM modulation, and complex positive-/negative-sequence extraction of grid voltage are not required. Ripples of active power or reactive power under unbalanced grid voltages are eliminated.

V. SIMULATION AND EXPERIMENTAL VERIFICATION

In order to verify the MPDPC control strategy with power compensation for fault-tolerant FSTP converter under unbalanced grid voltages, simulation and experiments are carried out. MATLAB simulation model is built with system parameters showing in Table III. The isolated transformer T is used to connect the bidirectional converter with power grid.

A. Simulation Results

Three-phase voltages are unbalanced with 20% voltage drop in phase B. Given active power changes from 1000 to -1000 W at 0.05 s. The simulation results of SSTP structure with conventional MPDPC and FSTP structure with MPDPC with power compensation are shown in Fig. 6. Both the current and output power are severely distorted and the converter cannot work properly with SSTP or conventional MPDPC control strategy,

TABLE III
SYSTEM PARAMETERS

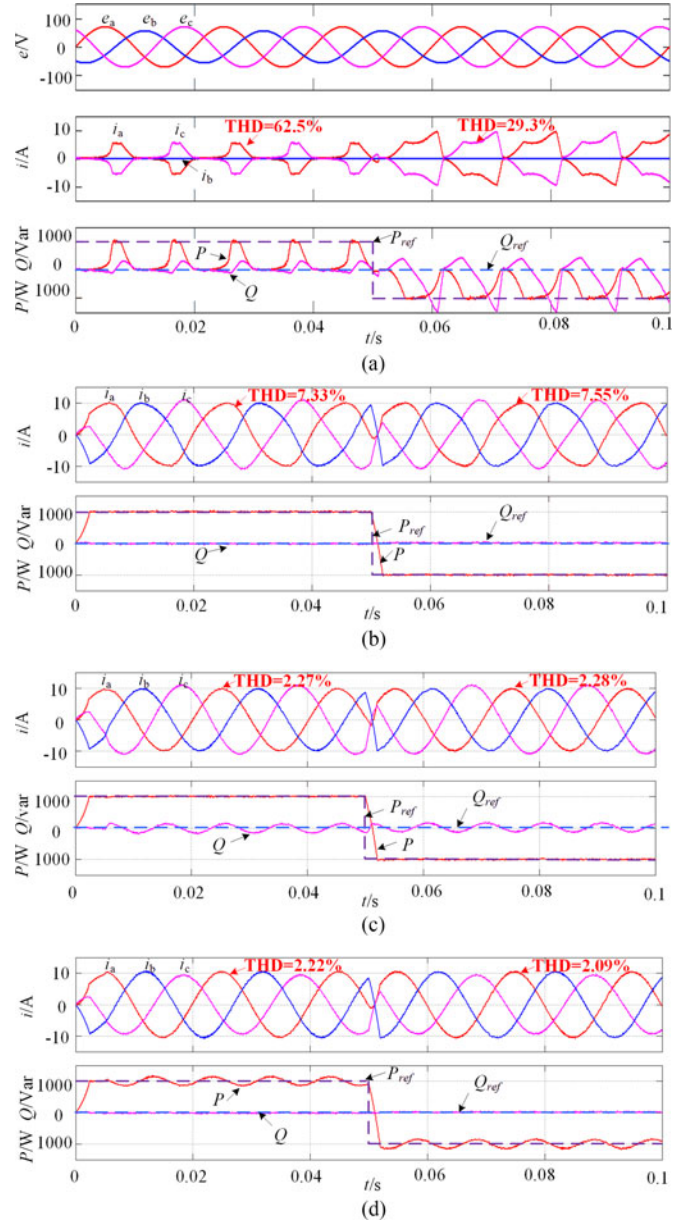| Symbol	System Parameters	Value
$U_{\rm dc}$	DC-side voltage	400 V
C	Capacitance	1500 μF
L	Filter inductance	20 mH
e	Power line voltage	380 V
f	Power line frequency	50 Hz
T	AC transformer	Y-Y, 380/50 V, 10 kVA
$f_{\rm samp}$	Sampling frequency	20 kHz

Fig. 6. Simulation results for switch fault of phase B when active power steps from 1000 to -1000 W under 20% voltage drop in phase B: (a) SSTP using MPDPC, (b) FSTP using MPDPC without power compensation, (c) FSTP MPDPC with power compensation I, and (d) FSTP MPDPC with power compensation II.
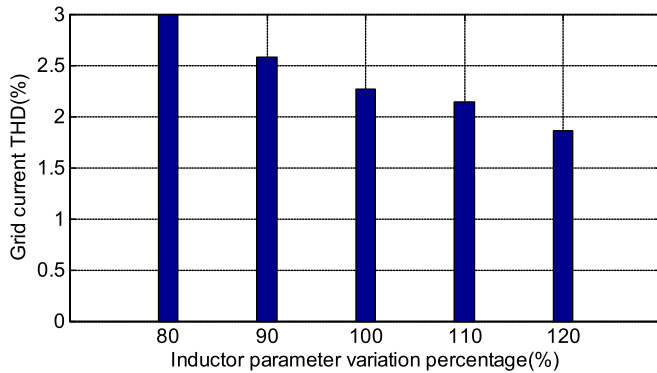
Fig. 7.   Grid current THD with filter inductor parameter variation.

Fig. 8.   Experimental setup.

which is shown in Fig. 6(a). The total harmonic distortion (THD) of grid currents is 62.5% in inverter mode and 29.3% in rectifier mode.

The output power can be controlled under FSTP MPDPC without power compensation, but the grid current has high distortion. As shown in Fig. 6(b), the current THD reaches 7.33% in inverter mode and 7.55% in rectifier mode, respectively. By comparison of the four control strategies, the current THD using the proposed FSTP MPDPC with power compensation I falls to 2.27% in inverter mode and 2.28% in rectifier mode and keeps active power constant without ripples, as shown in Fig. 6(c).

Under the control of FSTP MPDPC with power compensation II, the THD drops to 2.22% in inverter mode 2.09% in rectifier mode without reactive power ripples. The ripples in reactive power of Fig. 6(d) are eliminated and adjusted to reference values.

Simulation results show that the harmonic contents of grid current using FSTP MPDPC with power compensations I and II are smaller than using MPDPC without power compensation. The ripples in active power or reactive power can be eliminated. The conventional SSTP MPDPC method is invalid under unbalanced grid voltages.

B. Filter Parameter Robustness Simulation

The quality of the control strategy depends on the mathematic model to predict the voltage vector. The model errors have an effect over the power prediction. The dynamic vector equation of a grid current is

$$V = Ri + L\frac{di}{dt} + e \qquad (32)$$

where V, i, e are output voltage vector, current vector, grid voltage vector of the converter, respectively.

The load resistance R has a very small effect over the prediction and, in fact, it can be neglected. However, errors in inductance L have a major influence on the power prediction. In order to verify the impact of filter inductance on the control performance, simulation is designed with the actual filter parameter changing from 80% to 120% of the rated value. Fig. 7
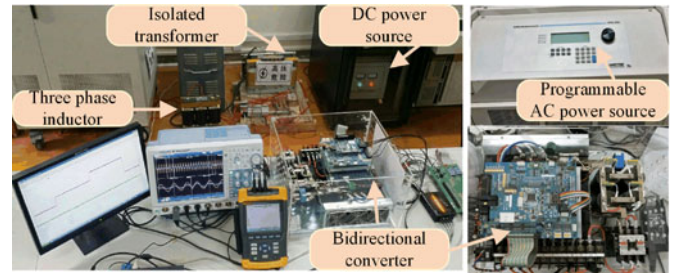
shows that THD of currents change from 2.99% to 1.86% with inductor parameter variation, which verifies the good robustness of the control system.

C. Experimental Results

In order to further verify the proposed control strategy performance, bidirectional ac/dc converter experimental setup based on PE-PRO is built as shown in Fig. 8. Control system is implemented by TI TMS320F28335 and IGBT 7MBP50RJ120. The test instrument is composed of YOKOGAWA DLM4000 series mixed-signal oscilloscope, FLUKE 435B power quality analyzer, and APL-II dc power supply. Amteke MX30 programmable ac power source is used to generate unbalanced grid voltage. The experimental parameters are shown in Table III.

The switch devices of phase B break down in converter operation and the grid voltage of phase B drops 20%. The steady-state experimental results of fault-tolerant converter with different control strategies are shown in Fig. 9. The reference power $p_{\rm ref}$ is 1000 W and $q_{\rm ref}$ is 0. The current of phase B drops to 0 and the current THD of other two phases reaches to 48.8% with SSTP in Fig. 9(a). The active and reactive power have large gap with the reference values.

In contrast, the results with FSTP MPDPC are better. The active and reactive power of FSTP without power compensation are kept stable in Fig. 9(b), but the THD of grid current is 7.7%, which cannot satisfy the grid requirements. The FSTP MPDPC with power compensation is proposed to improve the power quality. The grid current THD is reduced to 3.4% with power compensation I in Fig. 9(c) and 4.9% with power compensation II in Fig. 9(d). The ripples in active power and reactive power are eliminated, respectively. Furthermore, the dc voltage $U_{\rm dc}$ is stable and the capacitor neutral point voltage $U_C/2$ has small fluctuations. The results show the good performance of the proposed FSTP MPDPC in steady state with power compensation method under unbalanced grid voltages.

In order to verify the dynamic experimental performance when the switching devices of phase B have fault under 20% voltage drop in phase B, the reference active power steps from 1000 to -1000 W in Fig. 10. It is clearly seen that the waveform of the grid current using FSTP MPDPC with power compensation is sinusoidal and has lower THD, which is shown in Table IV. The constant active power and reactive power are achieved with power compensations I and II, respectively, as
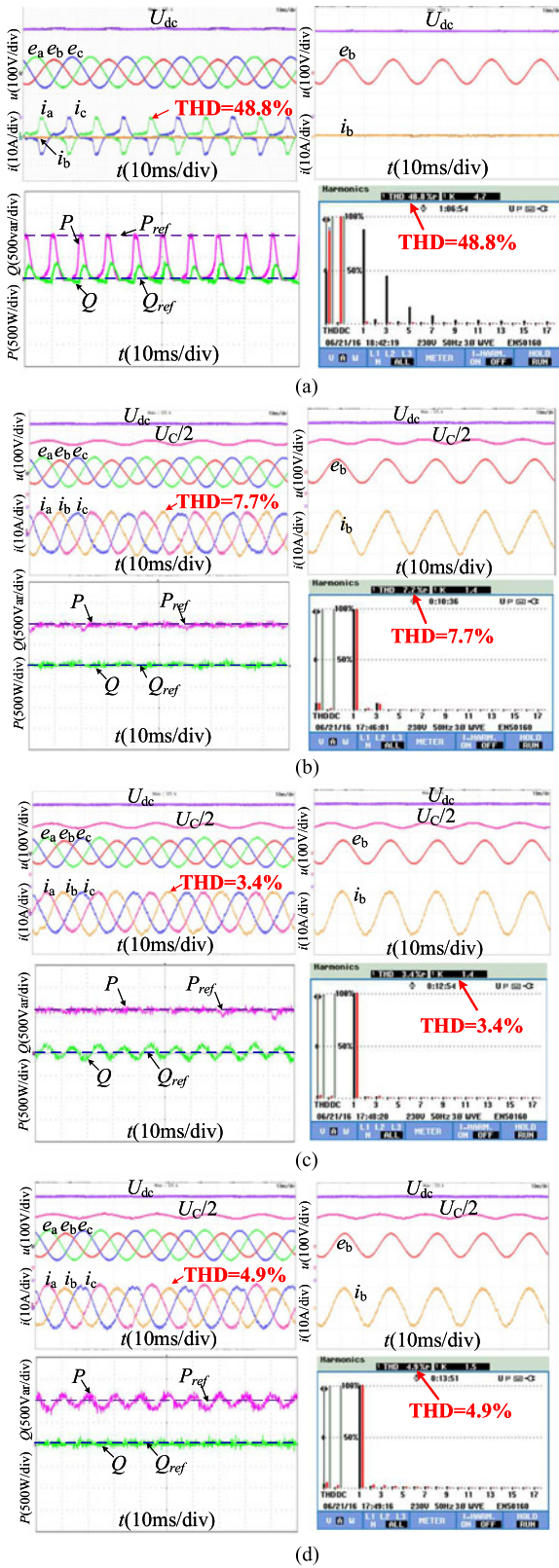
Fig. 9.   Steady-state experimental results for switch fault and 20% voltage drop in phase B: (a) SSTP structure using MPDPC method, (b) FSTP structure using MPDPC method, (c) FSTP structure using MPDPC with power compensation I, and (d) FSTP structure using MPDPC with power compensation II.
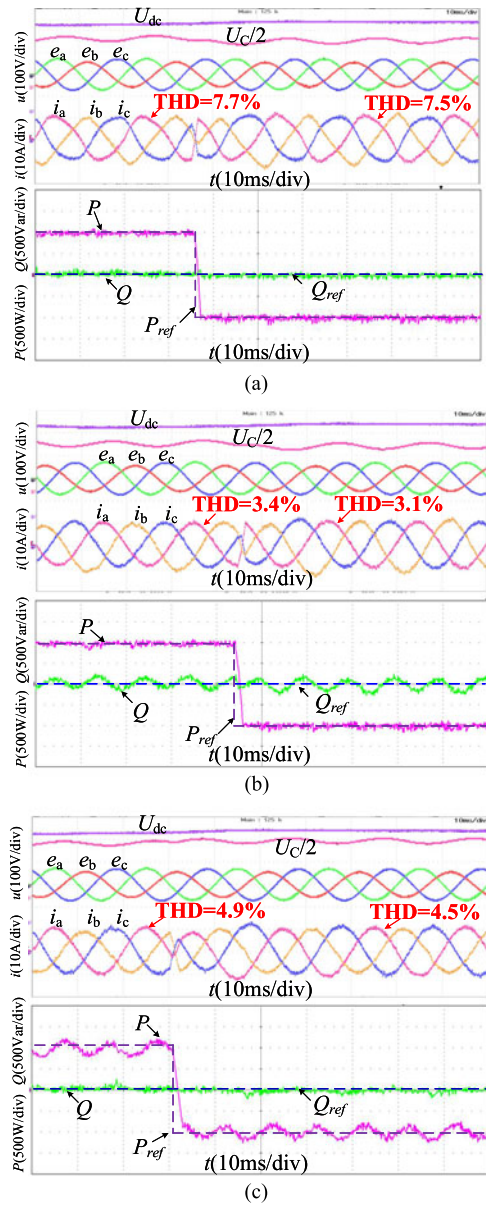

Fig. 10.   Dynamic experimental results for switch fault of phase B when active power steps from 1000 to −1000 W under 20% voltage drop in phase B: (a) FSTP structure using MPDPC method, (b) FSTP structure using MPDPC method with power compensation I, and (c) FSTP structure using MPDPC method with power compensation II.

shown in Fig. 10(b) and (c). On the contrary, the grid current of FSTP MPDPC without power compensation is highly distorted, as shown in Fig. 10(a). Besides, the dc voltage U_{dc} is stable and capacitor neutral point voltage $U_C/2$ has small fluctuations, which are the same to the simulation results. The experimental results confirm the effectiveness in the dynamic performance of the proposed FSTP MPDPC with power compensation method under unbalanced grid voltages.

From steady state and dynamic experimental results, the effectiveness of FSTP MPDPC with power compensations I and II are demonstrated. The power quality is improved with less

TABLE IV
THD OF GRID CURRENT

Condition	MPDPC	MPDPC with power compensation I	MPDPC with power compensation II
Inverter mode	7.7%	3.4%	4.9%
Rectifier mode	7.5%	3.1%	4.5%

current harmonics and twice grid-frequency ripples in active power or reactive power can be eliminated in fault-tolerant operation.

VI. CONCLUSION

In this paper, the structure of SSTP converter with switch fault was analyzed and the predictive power model of a fault-tolerant FSTP converter was established. Power compensations I and II were calculated by grid voltages and their 90° lagging signals in the $\alpha\beta$ stationary coordinate system without dq transform. FSTP MPDPC with power compensation strategy was designed to reduce current harmonics and eliminate the active or reactive power ripples.

The proposed control strategy can achieve the continuous operation of bidirectional ac/dc converter with switching devices fault under unbalanced grid voltages. This will enhance the reliability of the bidirectional ac/dc converter in weak microgrid. The PLL, PWM modulation, and traditional complex positive-/negative-sequence extractions of grid voltage are not required in this method. The effectiveness of the proposed method was validated by comparing the simulation and experimental results with different control strategies under unbalanced grid voltages.

REFERENCES

[1] P. Wang, C. Jin, D. Zhu, Y. Tang, P. C. Loh, and F. H. Choo, "Distributed control for autonomous operation of a three-port AC/DC/DS hybrid microgrid," *IEEE Trans. Ind. Electron.*, vol. 62, no. 2, pp. 1279–1290, Feb. 2015, doi: 10.1109/ TIE.2014.2347913.

[2] T. Ma, M. H. Cintuglu, and O. A. Mohammed, "Control of a hybrid AC/DC microgrid involving energy storage and pulsed loads," *IEEE Trans. Ind. Appl.*, vol. 53, no. 1, pp. 567–575, Jan./Feb. 2017, doi: 10.1109/TIA.2016.2613981.

[3] K. Sun, X. Wang, Y. W. Li, F. Nejabatkhah, Y. Mei, and X. Lu, "Parallel operation of bidirectional interfacing converters in a hybrid AC/DC microgrid under unbalanced grid voltage conditions," *IEEE Trans. Power Electron.*, vol. 32, no. 3, pp. 1872–1884, Mar. 2017, doi: 10.1109/TPEL.2016.2555140.

[4] Y. H. Liao and H. C. Chen, "Simplified PWM with switching constraint method to prevent circulating currents for paralleled bidirectional AC/DC converters in grid-tied system using graphic analysis," *IEEE Trans. Ind. Electron.*, vol. 62, no. 7, pp. 4573–4586, Jul. 2015, doi: 10.1109/TIE.2014.2352597.

[5] L. Gu and K. Jin, "A three-phase isolated bidirectional AC/DC converter and its modified SVPWM algorithm," *IEEE Trans. Power Electron.*, vol. 30, no. 10, pp. 5458–5468, Oct. 2015, doi: 10.1109/TPEL.2014.2378274.

[6] W. Zhang, D. Xu, P. N. Enjeti, H. Li, J. T. Hawke, and H. S. Krishnamoorthy, "Survey on fault-tolerant techniques for power electronic converters," *IEEE Trans. Power Electron.*, vol. 29, no. 12, pp. 6319–6331, Dec. 2014, doi: 10.1109/TPEL.2014.2304561.

[7] J. Fang, W. Li, H. Li, and X. Xu, "Online inverter fault diagnosis of buck-converter BLDC motor combinations," *IEEE Trans. Power Electron.*, vol. 30, no. 5, pp. 2674–2688, May 2015, doi: 10.1109/TPEL.2014.2330420.

[8] C. Cecati, A. O. D. Tommaso, F. Genduso, R. Miceli, and G. R. Galluzzo, "Comprehensive modeling and experimental testing of fault detection and management of a nonredundant fault-tolerant VSI," *IEEE Trans. Ind. Electron.*, vol. 62, no. 6, pp. 3945–3954, Jun. 2015, doi: 10.1109/TIE.2015.2402645.

[9] M. Pahlevani and P. Jain, "A fast DC-bus voltage controller for bidirectional single-phase AC/DC converters," *IEEE Trans. Power Electron.*, vol. 30, no. 8, pp. 4536–4547, Aug. 2015, doi: 10.1109/TPEL.2014.2356413.

[10] S. Eren, M. Pahlevani, A. Bakhshai, and P. Jain, "A digital current control technique for grid-connected AC/DC converters used for energy storage systems," *IEEE Trans. Power Electron.*, vol. 32, no. 5, pp. 3970–3988, May 2017, doi: 10.1109/TPEL.2016.2582901.

[11] H. Li, W. Li, and H. Ren, "Fault-tolerant inverter for high-speed low-inductance BLDC drives in aerospace applications," *IEEE Trans. Power Electron.*, vol. 32, no. 3, pp. 2452–2463, Mar. 2017, doi: 10.1109/TPEL.2016.2569611.

[12] K. D. Hoang, Z. Q. Zhu, and M. P. Foster, "Influence and compensation of inverter voltage drop in direct torque-controlled four-switch three-phase PM brushless AC drives," *IEEE Trans. Power Electron.*, vol. 26, no. 8, pp. 2343–2357, Aug. 2011, doi: 10.1109/TPEL.2010.2096561.

[13] R. Wang, J. Zhao, and Y. Liu, "A comprehensive investigation of four-switch three-phase voltage source inverter based on double Fourier integral analysis," *IEEE Trans. Power Electron.*, vol. 26, no. 10, pp. 2774–2787, Oct. 2011, doi: 10.1109/TPEL.2011.2119381.

[14] S. Dasgupta, S. N. Mohan, S. K. Sahoo, and S. K. Panda, "Application of four-switch-based three-phase grid-connected inverter to connect renewable energy source to a generalized unbalanced microgrid system," *IEEE Trans. Ind. Electron.*, vol. 60, no. 3, pp. 1204–1215, Mar. 2013, doi: 10.1109/TIE.2012. 2202350.

[15] M. S. Diab, A. Elserougi, A. M. Massoud, A. S. Abdel-Khalik, and S. Ahmed, "A four-switch three-phase SEPIC-based inverter," *IEEE Trans. Power Electron.*, vol. 30, no. 9, pp. 4891–4905, Sep. 2015, doi: 10.1109/TPEL.2014.2363853.

[16] D. Zhou, J. Zhao, and Y. Liu, "Predictive torque control scheme for three-phase four-switch inverter-fed induction motor drives with DC-Link voltages offset suppression," *IEEE Trans. Power Electron.*, vol. 30, no. 6, pp. 3309–3318, Jun. 2015, doi: 10.1109/TPEL.2014.2338395.

[17] C. Hung-Chi and L. Jhen-Yu, "Bidirectional current sensorless control for the full-bridge AC/DC converter with considering both inductor resistance and conduction voltages," *IEEE Trans. Power Electron.*, vol. 29, no. 4, pp. 2071–2082, Apr. 2014, doi: 10.1109/TPEL.2013.2265323.

[18] Y. H. Liao, "A novel reduced switching loss bidirectional AC/DC converter PWM strategy with feedforward control for grid-tied microgrid systems," *IEEE Trans. Power Electron.*, vol. 29, no. 3, pp. 1500–1513, Mar. 2014, doi: 10.1109/TPEL.2013.2260872.

[19] K. Ma, W. Chen, M. Liserre, and F. Blaabjerg, "Power controllability of a three-phase converter with an unbalanced AC source," *IEEE Trans. Power Electron.*, vol. 30, no. 3, pp. 1591–1604, Mar. 2015, doi: 10.1109/TPEL.2014.2314416.

[20] J. Miret, M. Castilla, A. Camacho, L. G. d. Vicuña, and J. Matas, "Control scheme for photovoltaic three-phase inverters to minimize peak currents during unbalanced grid-voltage sags," *IEEE Trans Power Electron.*, vol. 27, no. 10, pp. 4262–4271, Oct. 2012, doi: 10.1109/TPEL.2012.2191306.

[21] H. Nian, Y. Shen, H. Yang, and Y. Quan, "Flexible grid connection technique of voltage-source inverter under unbalanced grid conditions based on direct power control," *IEEE Trans. Ind. Appl.*, vol. 51, no. 5, pp. 4041–4050, Sep./Oct. 2015, doi: 10.1109/TIA.2015.2428219.

[22] L. Shang, D. Sun, and J. Hu, "Sliding-mode-based direct power control of grid-connected voltage-sourced inverters under unbalanced network conditions," *IET Power Electron.*, vol. 4, no. 5, pp. 570–579, Aug. 2011, doi: 10.1049/iet-pel.2010. 0160.

[23] Y. Zhang and C. Qu, "Model predictive direct power control of PWM rectifiers under unbalanced network conditions," *IEEE Trans. Ind. Electron.*, vol. 62, no. 7, pp. 4011–4022, Oct. 2015, doi: 10.1109/TIE.2014.2387796.

[24] D. Sun and X. Wang, "Low-complexity model predictive direct power control for DFIG under both balanced and unbalanced grid conditions," *IEEE Trans. Ind. Electron.*, vol. 63, no. 8, pp. 5186–5196, Aug. 2016, doi: 10.1109/TIE. 2016.2570201.

[25] J. Alonso-Martínez, J. E. G. Carrasco, and S. Arnaltes, "Table-based direct power control: A critical review for microgrid applications," *IEEE Trans. Power Electron.*, vol. 25, no. 12, pp. 2949–2961, Dec. 2010, doi: 10.1109/TPEL.2010. 2087039.

[26] Y. Zhang and J. Zhu, "Direct torque control of permanent magnet synchronous motor with reduced torque ripple and commutation frequency," *IEEE Trans. Power Electron.*, vol. 26, no. 1, pp. 235–248, Jan. 2011, doi: 10.1109/ TPEL.2010.2059047.

[27] S. Sajadian and R. Ahmadi, "Model predictive-based maximum power point tracking for grid-tied photovoltaic applications using a Z-source inverter," *IEEE Trans. Power Electron.*, vol. 31, no. 11, pp. 7611–7620, Nov. 2016, doi: 10.1109/TPEL.2016.2537814.

[28] J. Yang, W. X. Zheng, S. Li, B. Wu, and M. Cheng, "Design of a prediction-accuracy-enhanced continuous-time MPC for disturbed systems via a disturbance observer," *IEEE Trans. Ind. Electron.*, vol. 62, no. 9, pp. 5807–5816, Sep. 2015, doi: 10.1109/TIE.2015.2450736.

[29] F. Zhang, W. Li, and G. Joós, "A voltage-level-based model predictive control of modular multilevel converter," *IEEE Trans. Ind. Electron.*, vol. 63, no. 8, pp. 5301–5312, Aug. 2016, doi: 10.1109/TIE.2016.2572671.

[30] Y. Zhang, X. Wu, X. Yuan, Y. Wang, and P. Dai, "Fast model predictive control for multilevel cascaded H-bridge STATCOM with polynomial computation time," *IEEE Trans. Ind. Electron.*, vol. 63, no. 8, pp. 5231–5243, Aug. 2016, doi: 10.1109/TIE.2016.2572662.

[31] J. Rodriguez *et al.*, "State of the art of finite control set model predictive control in power electronics," *IEEE Trans. Ind. Informat.*, vol. 9, no. 2, pp. 1003–1016, May 2013, doi: 10.1109/TII.2012.2221469.

[32] B. S. Riar, T. Geyer, and U. K. Madawala, "Model predictive direct current control of modular multilevel converters: Modeling, analysis, and experimental evaluation," *IEEE Trans. Power Electron.*, vol. 30, no. 1, pp. 431–439, Jan. 2015, doi: 10.1109/TPEL.2014.2301438.

[33] V. Yaramasu, B. Wu, and J. Chen, "Model-predictive control of grid-tied four-level diode-clamped inverters for high-power wind energy conversion systems," *IEEE Trans. Power Electron.*, vol. 29, no. 6, pp. 2861–2873, Jun. 2014, doi: 10.1109/TPEL.2013.2276120.

[34] J. Hu, J. Zhu, and D. G. Dorrell, "Model predictive control of grid-connected inverters for PV systems with flexible power regulation and switching frequency reduction," *IEEE Trans. Ind. Appl.*, vol. 51, no. 1, pp. 587–594, Jan./Feb. 2015, doi: 10.1109/TIA.2014.2328785.

[35] I. M. B. Hassine, M. W. Naouar, and N. Mrabet-Bellaaj, "Model predictive-sliding mode control for three-phase grid-connected converters," *IEEE Trans. Ind. Electron.*, vol. 64, no. 2, pp. 1341–1349, Feb. 2017, doi: 10.1109/TIE. 2016.2618867.

Shiyang Hu received the M.S. degree in electrical engineering from Zhengzhou University of Light Industry, Zhengzhou, China, in 2016. He is currently working toward the Ph.D. degree in the College of Electrical and Information Engineering, Hunan University, Changsha, China.

He is mainly involved in technology on renewable energy power generation, intelligent control methods of converters, and wind power forecasting.

Chun Gan (S'14–M'16) received the B.S. and M.S. degrees from the China University of Mining and Technology, Jiangsu, China, in 2009 and 2012, respectively, and the Ph.D. degree from Zhejiang University, Hangzhou, China, in 2016, all in power electronics and motor drives.

He is currently a Research Associate in the Department of Electrical Engineering and Computer Science, The University of Tennessee, Knoxville, TN, USA. He has published more than 30 technical papers in leading journals and conference proceedings. His research interests include high-efficiency power converters, high-voltage direct current transmission, microgrids, electrical motor drives, and electrical motor design.

Dr. Gan received the 2015 Top Ten Excellent Scholar Award, the 2016 Excellent Ph.D. Graduate Award, the 2015 Ph.D. National Scholarship, the 2015 Wang Guosong Scholarship, and the 2014 and 2015 Outstanding Ph.D. Candidate Awards from Zhejiang University.

Nan Jin (M'16) received the B.S. and M.S. degrees in electrical engineering from Zhengzhou University of Light Industry, Zhengzhou, China, in 2003 and 2007, respectively, and the Ph.D. degree in power electronics and electrical drives from Shanghai Jiao Tong University, Shanghai, China, in 2012.

He is currently an Associate Professor with Zhengzhou University of Light Industry. He is also a Visiting Professor in the Department of Electrical Engineering and Computer Science, The University of Tennessee, Knoxville, TN, USA. He has published more than 30 technical papers in journals and conference proceedings, two books, and hold eight Chinese patents. His research interests include model predictive control method for power converters, fault diagnosis, and tolerant control of power electronics systems.

Zhibin Ling (M'12) received the B.S. and M.S. degrees from Harbin Science and Technology University, Harbin, China, in 1997 and 2000, respectively, and the Ph.D. degree from Shanghai Jiao Tong University, Shanghai, China, in 2004, all in electrical engineering.

He has been with Shanghai Jiao Tong University since 2004, where he is currently an Associate Professor. He has been PI of externally funded research sponsored by the National Natural Science Foundation of China, Ministry of Science and Technology, and several utilities. He has authored more than 50 technical articles, one book chapter, and has obtained 15 patents. His research interests include battery energy storage, renewable power generation, ac/dc hybrid power grids, dc grids, and power electronics applications in power systems.